NASA Technical Memorandum 106474

Turbulence Models and Reynolds Analogy for Two-Dimensional Supersonic Compression Ramp Flow

Chi R. Wang
Lewis Research Center
Cleveland, Ohio

and

Maleina C. Bidek
Cornell University
Ithaca, New York

Prepared for the
1994 Thermophysics and Heat Transfer Conference
sponsored by the American Society of Mechanical Engineers
Colorado Springs, Colorado, June 20–23, 1994

NASA

TURBULENCE MODELS AND REYNOLDS ANALOGY FOR TWO-DIMENSIONAL SUPERSONIC COMPRESSION RAMP FLOW

Chi R. Wang
National Aeronautics and Space Administration
Lewis Research Center
Cleveland, Ohio 44135

and

Maleina C. Bidek[1]
Cornell University
Ithaca, New York 14853

ABSTRACT

We present results of the application of turbulence models and the Reynolds analogy to the Navier-Stokes computations of Mach 2.9 two-dimensional compression ramp flows. We studied the Baldwin-Lomax eddy viscosity model and the $k-\varepsilon$ turbulence transport equations for the turbulent momentum flux modeling in the Navier-Stokes equations. We also studied the Reynolds analogy for the turbulent heat flux modeling in the energy equation. The Navier-Stokes equations and the energy equation were numerically solved for the flow properties. The Reynolds shear stress, the skin friction factor, and the surface heat transfer rate were calculated and compared with their measurements. We concluded that (a) with a hybrid $k-\varepsilon$ turbulence model for turbulence modeling, the present computations predicted the skin friction factors of the 8° and 16° compression ramp flows and (b) with the turbulent Prandtl number Pr_t = 0.93 and the ratio of the turbulent thermal and momentum transport coefficients $\mu_q / \mu_t = 2 / \mathrm{Pr}_t$, the present computations also predicted the surface heat transfer rates beneath the boundary layer flow of the 16° compression ramp.

NOMENCLATURES

C_f	skin friction factor, $\tau_w / (1/2)\rho_\infty U_\infty^2$
$C_i, C_o, C_{kleb}, C_\mu, C_s$	sempirical constants
C_p	specific heat
K	thermal conductivity
k	turbulence kinetic energy
n	direction normal to wall surface
p	static pressure
Pr_ℓ	laminar Prandtl number, 0.73
Pr_t	turbulent Prandtl number, 0.93
Q	thermal flux
Re	Reynolds number, $\rho_\infty U_\infty \delta_0 / \mu_\infty$
S	Reynolds analogy factor, $\left(\mu_q / \mu_t\right)\mathrm{Pr}_t$
T	static temperature
t	time
t'	temperature fluctuation
U	X-direction velocity component
U_τ	frictional velocity, $\left(\mu_w \lvert\omega\rvert_w / \rho_w\right)^{0.5}$
U_s	velocity component parallel to wall surface
u'	X-direction velocity fluctuation
V	Y-direction velocity component
v'	Y-direction velocity fluctuation
X,Y	physical coordinates

[1] Student intern at NASA Lewis Research Center.

Y^+	$(\rho_w \lvert\omega\rvert_w / \mu_w)^{0.5} Y$
δ	boundary layer thickness
δ_{ij}	Kronecker delta
ε	turbulence dissipation rate
μ	dynamic viscosity
μ_q	turbulent thermal transport coefficient
μ_t	turbulent eddy viscosity
ρ	density
τ_w	surface shear stress
τ_{XY}	Reynolds shear stress, $\mu_t(\partial U / \partial Y + \partial V / \partial X)$
ω	vorticity

Subscripts

c	condition at ramp corner
d	downstream of ramp corner
s	sublayer condition
u	upstream of ramp corner
v	sublayer edge condition
w	wall surface condition
o	condition at $X = 0$
∞	free stream condition
o,∞	free stream stagnation condition

Superscript

-	incompressible flow condition

INTRODUCTION

Shock wave/turbulent boundary layer interaction flow is an important phenomenon which occurs in the flow field of a high speed propulsion inlet system. A review of the existing literature on the shock wave/boundary layer interaction flows can be found in an AGARD report [1]. Generally, the existing studies have described the flow phenomena for transonic and supersonic speed regions by using experimental observations, correlations, theoretical concepts, and numerical solutions of the compressible Navier-Stokes equations. Existing computational studies [2 and 3] indicate that, with proper turbulence models, solutions of the Navier-Stokes equations and the energy equation could predict the surface pressure and skin friction variations for most of the interaction flows.

The surface heat transfer within the shock wave/boundary layer interaction flow is also very important to the design of a high speed propulsion inlet system. For many turbulent flow analyses, a practical approach to estimate the turbulence effect on the surface heat transfer has been the Reynolds analogy. However, boundary layer theory [4] indicates that the use of Reynolds analogy requires a wide range of turbulent Prandtl numbers in order to properly model the turbulent thermal fluxes in pipe flow and a heated boundary layer flow. Closer to the present work, a recent experiment [5] of a supersonic compression ramp flow also revealed that the Reynolds analogy needed an additional factor to correlate the Stanton number and the local skin friction factor. Therefore, there is a need to investigate the application of the Reynolds analogy for the modeling of the turbulent thermal flux within a shock wave/turbulent boundary layer interaction flow field.

The present paper describes some Navier-Stokes computational analyses of the Reynolds shear stresses and the surface heat transfer in a two-dimensional shock wave/turbulent boundary layer interaction flow. We considered the shock wave/boundary layer interaction around 8° and 16° compression ramps (Fig. 1) imbedded in a fully developed turbulent boundary layer flow. The free stream Mach number was 2.9. The free stream Reynolds number (based on the initial boundary layer thickness δ_o) was 1.7×10^6. These are the experimental conditions of Ref. [5]. The Baldwin-Lomax turbulence model [6], the low Reynolds number $k-\varepsilon$ turbulence model of Nichols [7] and their revised versions [8] were each used, respectively, to model the turbulent momentum fluxes in the momentum equation. The Reynolds analogy was then used to model the turbulent heat flux in the energy equation. The turbulent Prandtl number was constant and equal to 0.93. The turbulent thermal flux was represented by the product of the mean temperature gradient and a transport coefficient. A Reynolds analogy factor was used to account for the stream-wise variation of the ratio of the thermal trans-

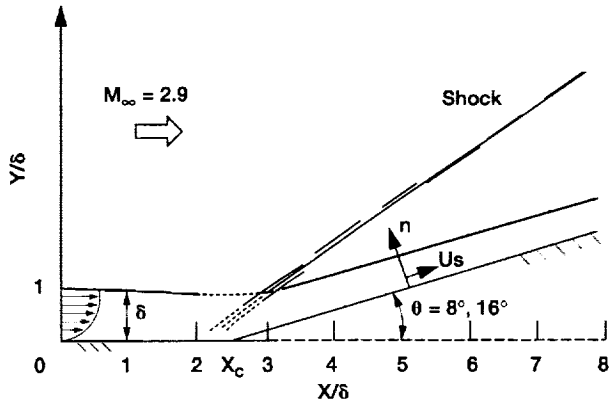

Figure 1.—Compression ramp flow model (δ_o = 26 mm, $Re = \rho_\infty U_\infty \delta_o / \mu_\infty = 1.76 \times 10^6$).

port coefficient and the turbulent eddy viscosity. The compressible Navier-Stokes equations and the energy equation were solved for the flow properties with a time-dependent explicit finite difference computational code [9].

The present Navier-Stokes computational results of the turbulent eddy viscosity, the Reynolds shear stress, the mean flow velocity, and the surface heat transfer rate within the interaction flow fields are described and compared with their measurements in the existing experiments [5, 10, and 11]. Based on the comparisons, the effectiveness of the turbulence modeling techniques and the Reynolds analogy on the predictions of the Reynolds shear stress, the skin friction factor, the surface pressure, and the surface heat transfer rate of the supersonic compression ramp flow are discussed in the paper.

TURBULENCE MODELS

The Baldwin and Lomax model [6] is widely used for turbulence modeling in compressible flows. A compressible $k-\varepsilon$ two equation turbulence model developed by Nichols has been used in some supersonic flow computations [7]. Viscous sublayer turbulence models [12 and 13] have been developed and incorporated with the k and ε equations to resolve the near wall turbulence modeling. Previous studies [7, 12, and 13] presented the applications of the $k-\varepsilon$ turbulence model and the viscous sublayer turbulence models in the predictions of the surface pressure and skin frictions of compression ramp flows with large deflection angle and free stream Mach number. The effectiveness of these models on the computations of the Reynolds shear stress and the surface heat transfer rate within a compression ramp flow were not reported.

In the present work, we studied the existing turbulence modeling techniques [6, 7, 12, and 13] for the computations of the Reynolds shear stresses and surface heat transfer rates of two-dimensional compression ramp flows (Fig. 1). Two flow fields with different deflection angles (8° and 16°) were considered. Experiments [10] of the flow fields indicated that flow separation did not occur. Thus, we did not consider the turbulence modeling of a separated flow. A summary of the turbulence modeling techniques used here is given in the following section.

Baldwin and Lomax Turbulence Model

This turbulence model is a two-layer eddy viscosity model. The eddy viscosity formulas of a two-dimensional flat plate turbulent boundary layer flow are shown in the following:
In the inner layer, the eddy viscosity, $\mu_{t,i}$, is described by

$$\mu_{t,i}=\rho\left[C_i Y\left(1-e^{-Y^+/26}\right)\right]^2|\omega| \qquad (1)$$

where

$$Y^+=\left(\rho_w|\omega_w|/\mu_w\right)^{0.5}Y \quad \text{and} \quad |\omega|=\sqrt{\left(\frac{\partial U}{\partial Y}-\frac{\partial V}{\partial X}\right)^2}$$

In the outer layer, the eddy viscosity, $\mu_{t,o}$, is described by

$$\mu_{t,o}=0.0168\ C_o\rho F_{\text{wake}}F_{\text{kleb}} \qquad (2)$$

F_{wake} is the smaller of $Y_{\max}F_{\max}$ and $0.25\ Y_{\max}U_{\max}^2/F_{\max}$,

$$U_{\max}=\left(\sqrt{U^2+V^2}\right)_{\max}, \text{ and } \quad F=Y|\omega|\left(1-e^{-Y^+/26}\right)$$

The quantity, $F_{\max}$, is the maximum value of F that occurs in a profile and $Y_{\max}$ is the value of Y at which $F_{\max}$ occurs. The function, F_{kleb}, is the Klebanoff intermittency factor given by

$$F_{\text{kleb}}=\frac{1}{1+5.5\left(C_{\text{kleb}}Y/Y_{\max}\right)^6} \qquad (3)$$

In earlier work [8], the empirical constants, C_i, C_o, and C_{kleb}, appearing in Eqs. (1) to (3) were adjusted to achieve better prediction of the Reynolds shear stress in the supersonic compression ramp flow field. Different sets of these empirical constants were found to model the turbulence eddy viscosity upstream and downstream of the compression ramp. These sets of empirical constants are (1) C_i = 0.41, C_o = 1, and C_{kleb} = 0.8 for the upstream modeling, $X \le X_c$ and (2) C_i = 0.45, C_o = 2, and C_{kleb} = 0.8 for the downstream modeling, $X > X_c$. Using these empirical constants, we modified the Clauser constant and the Klebanoff intermittency factor of the Baldwin-Lomax turbulence model.

$k-\varepsilon$ Turbulence Models

The following compressible low Reynolds number turbulence model was first used [7] to predict the turbulent eddy viscosity within the supersonic flat plate turbulent boundary layer flow.

The turbulent eddy viscosity, μ_t, was defined as

$$\mu_t=\rho C_\mu\left(\frac{k^2}{\varepsilon}\right)\left(1-e^{-0.0115\rho U_\tau/\mu}\right) \qquad (4)$$

with C_μ = 0.09.
The turbulence kinetic energy, k, and the dissipation rate, ε, were described by using the following transport equations:

$$\frac{\partial}{\partial t}(\rho k)+\frac{\partial}{\partial X}(\rho U k)+\frac{\partial}{\partial Y}(\rho V k)=\frac{\partial}{\partial X}\left[(\mu+\mu_t)\frac{\partial k}{\partial X}\right]+\frac{\partial}{\partial Y}\left[(\mu+\mu_t)\frac{\partial k}{\partial Y}\right]+P-\rho\varepsilon-\frac{2\mu k}{Y^2} \qquad (5)$$

$$\frac{\partial}{\partial t}(\rho\varepsilon)+\frac{\partial}{\partial X}(\rho U\varepsilon)+\frac{\partial}{\partial Y}(\rho V\varepsilon)$$
$$=\frac{\partial}{\partial X}\left[\left(\mu+\frac{\mu_t}{1.3}\right)\frac{\partial\varepsilon}{\partial X}\right]+\frac{\partial}{\partial Y}\left[\left(\mu+\frac{\mu_t}{1.3}\right)\frac{\partial\varepsilon}{\partial Y}\right]$$
$$+1.35\frac{\varepsilon P}{k}-\frac{\varepsilon}{k}\left(1.8f\rho\varepsilon+\frac{2\mu k e^{-0.5\rho U_\tau Y/\mu}}{Y^2}\right) \quad (6)$$

where

$$f=1-\frac{0.2}{0.9}e^{-\left(k^2\rho/6\mu\varepsilon\right)^2} \quad (7)$$

The production term, P, was defined as

$$P=\left\{\mu_t\left[\left(\frac{\partial U_i}{\partial X_j}+\frac{\partial U_j}{\partial X_i}\right)-\frac{2}{3}\delta_{ij}\frac{\partial U_k}{\partial X_k}\right]-\frac{2}{3}\rho k\delta_{ij}\right\}\frac{\partial U_i}{\partial X_j} \quad (8)$$

Equations (4) to (8) were also solved for the turbulent eddy viscosity in the computations of the interaction flow along the compression ramp. The source terms were found to be numerically stiff at locations near the corner of the compression ramp. Therefore, a viscous sublayer model [12] was used to eliminate the stiffness problem. This viscous sublayer model and the high Reynolds number forms of the $k-\varepsilon$ turbulence model corresponding to Eqs. (4) to (8) were combined to formulate the following hybrid $k-\varepsilon$ turbulence model [8] for the flow over the compression ramp.

Adjacent to the wall, the viscous sublayer thickness, Y_v, was defined by

$$Y_v=20\left(\frac{\mu_w}{\rho_w}\right)\left(\frac{C_s^{0.25}}{U_\tau}\right) \quad (9)$$

where C_s (= 0.4) is an empirical constant. Within the viscous sublayer thickness, $0 < Y \le Y_v$, the turbulent eddy viscosity, $\mu_{t,s}$, was expressed as

$$\mu_{t,s}=\left\{C_\mu+\left[0.8\left(\frac{C_\mu}{C_s^{0.5}}\right)\left(\frac{\rho_v}{\rho_w}\right)^{0.5}-C_\mu\right]\frac{Y}{Y_v}\right\}\left(\frac{\rho}{Y^+}\right)\frac{k_s^2}{\varepsilon_s} \quad (10)$$

where the turbulence kinetic energy, k_s, and the dissipation rate, ε_s, are

$$k_s=\left(\frac{\rho_v}{\rho}\right)k_v\left(\frac{Y}{Y_v}\right)^2 \quad (11)$$

and

$$\varepsilon_s=2\left(\frac{\mu_w}{\rho_w}\right)\left(\frac{k_v}{Y_v^2}\right) \quad (12)$$

k_v and ε_v are the turbulence kinetic energy and its dissipation rate at the viscous sublayer edge. They are

$$k_v=\left(\frac{U_\tau^2}{C_s^{0.5}}\right)\left(\frac{\rho_w}{\rho_v}\right) \quad (13)$$

and

$$\varepsilon_v=\left(\frac{U_\tau^3}{0.4Y_v}\right)\left(\frac{\rho_w}{\rho_v}\right)^{1.5} \quad (14)$$

At locations outside of the viscous sublayer, the high-Reynolds-number forms of Eqs. (4) to (8) were solved for the eddy viscosity. The free stream turbulence kinetic energy and the dissipation rate were the far field boundary conditions. Similar turbulence quantities given by Eqs. (13) and (14) were the boundary conditions at the viscous sublayer edge.

REYNOLDS ANALOGY

The general and practical heat transfer modeling technique for a turbulent flow is the Reynolds analogy. Given a turbulent Prandtl number, the analogy relates the turbulent thermal flux to the turbulent momentum flux. In this section, we describe the application of the Reynolds analogy in the prediction of the surface heat transfer downstream of the compression ramp flow.

We postulate that the turbulent thermal fluxes, $\rho\overline{u't'}$ and $\rho\overline{v't'}$ assume the forms

$$\rho\overline{u't'}=-\mu_q\frac{\partial T}{\partial X} \quad (15)$$

and

$$\rho\overline{v't'}=-\mu_q\frac{\partial T}{\partial Y} \quad (16)$$

where μ_q is the thermal transport coefficient. Including the thermal conduction fluxes, the total thermal fluxes in X and Y directions are

$$Q_x=-K\frac{\partial T}{\partial X}-C_p\mu_q\frac{\partial T}{\partial X} \quad (17)$$

and

$$Q_y=-K\frac{\partial T}{\partial Y}-C_p\mu_q\frac{\partial T}{\partial Y} \quad (18)$$

Introducing the laminar Prandtl number, $\mathrm{Pr}_\ell = C_p \mu / K$, into Eqs. (17) and (18), the thermal heat flux terms become

$$Q_x = -C_p\left(\frac{\mu}{\mathrm{Pr}_\ell}\frac{\partial T}{\partial X} + \frac{\mu_q}{\mu_t}\mu_t\frac{\partial T}{\partial X}\right) \tag{19}$$

and

$$Q_y = -C_p\left(\frac{\mu}{\mathrm{Pr}_\ell}\frac{\partial T}{\partial Y} + \frac{\mu_q}{\mu_t}\mu_t\frac{\partial T}{\partial Y}\right) \tag{20}$$

The ratio, μ_t / μ_q, is usually called the turbulent Prandtl number, Pr_t. In a turbulent pipe flow study [4] it was found that the ratio, μ_q / μ_t, varied from about 1 at near wall location to about 1.5 at the pipe center. Another study [4] of a boundary layer on a heated wall also revealed that the ratio, μ_q / μ_t, increased from about 1 at the near wall location to approximately 2 at the boundary layer edge. Thus, the ratio, μ_q / μ_t, is usually assumed to have a value of 1 at near wall locations. The above results were obtained from incompressible turbulent flow investigations.

An experiment [5] was recently performed to study the heat transfer of a shock wave/turbulent boundary layer interaction flow. The interaction flow field generated by a 16° compression ramp in a Mach 2.84 flow was considered. The results (Fig. 2) show the Reynolds analogy factor (the ratio of the Stanton number and half of the skin friction factor) increased, significantly at the downstream locations. The factor appeared to level-off at a value of 2.15 at the downstream location. This may imply that μ_q / μ_t may be greater than 1 at near wall locations downstream of the compression flow field.

Based on the above observations, we propose that, for the compression ramp flow the conventional definitions must be modified,

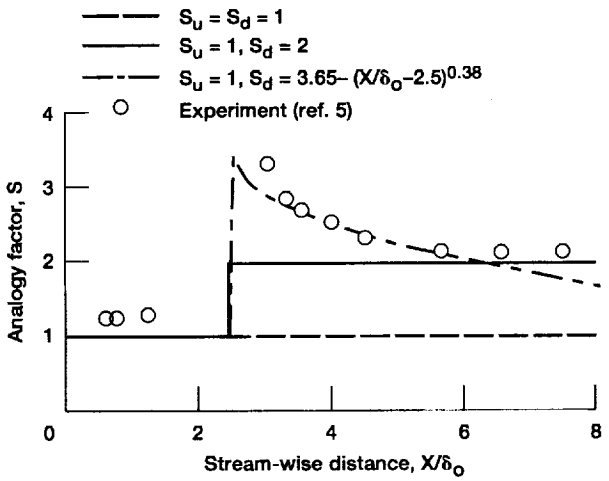

Figure 2.—Reynolds analogy factor, θ = 16°.

$$\frac{\mu_q}{\mu_t} = \frac{S}{\mathrm{Pr}_t} \tag{21}$$

where S is the Reynolds analogy factor. Introducing Eq. (21) into Eqs. (19) and (20), we obtained the following expressions

$$Q_x = -C_p\left(\frac{\mu}{\mathrm{Pr}_\ell}\frac{\partial T}{\partial X} + \frac{S\mu_t}{\mathrm{Pr}_t}\frac{\partial T}{\partial X}\right) \tag{22}$$

and

$$Q_Y = -C_p\left(\frac{\mu}{\mathrm{Pr}_\ell}\frac{\partial T}{\partial Y} + \frac{S\mu_t}{\mathrm{Pr}_t}\frac{\partial T}{\partial Y}\right) \tag{23}$$

for the thermal fluxes. We further assumed that S only varies along the X-direction. As shown in Fig. 2, three different potential analogy factor variations, S as function of X / δ_o, were considered in this study;

1. The analogy factor is constant, $S = 1$.
2. A discontinuity in S occurs at the corner $X / \delta_o = X_c / \delta_o$. S is 1 at upstream locations and S changes to a value of 2 at downstream locations.
3. A discontinuity in S occurs at the corner $X / \delta_o = X_c / \delta_o$. S is 1 at the upstream locations $\left(X / \delta_o < X_c / \delta_o\right)$. At the downstream locations, S varies approximately following the ratio of the Stanton number and the skin friction factor from the experiment [5].

In the present study, the Baldwin-Lomax eddy viscosity formulas and the $k - \varepsilon$ turbulence models were first used to model the turbulent momentum fluxes in the Navier-Stokes equations. Then, the above Reynolds analogy, with $\mathrm{Pr}_t = 0.93$, was used to model the thermal flux in the energy equation. Numerical computations were performed to solve the transport equations. Since the surface heat transfer measurements were only available for the 16° compression ramp flow, the heat transfer portion of the present computational analysis was also limited to the 16° compression flow field.

COMPUTATIONAL METHODS

The mass averaged unsteady compressible turbulent Navier-Stokes equations and the energy equation were solved numerically for the steady state properties within the compression ramp flows. These properties are the density, ρ, the velocity components, U and V, and the static temperature, T. The equation of state for an ideal gas was used to calculate the static pressure, p. The turbulent eddy viscosity, μ_t, was calculated, with or without the turbulence quantities, k and ε, based on the selection of the turbulence modeling technique. These properties were then used to compute the Reynolds shear stress, τ_{XY}, skin friction factor, C_f, and the surface heat transfer, Q_w.

A time-dependent explicit numerical computational method was used. Shang et al. [9] developed such a computational code, using MacCormack's finite difference scheme [14]. This code used the standard Baldwin-Lomax eddy viscosity concept to model the turbulence terms. This code was revised by modifying the Baldwin-Lomax eddy viscosity concept and by adding the present $k-\varepsilon$ turbulence models as described in the section TURBULENCE MODELS. The revised code with four models available was used for the present computations. The conservation equations, the coordinate transformations between the physical and the computational domains, and the finite difference scheme used in the numerical computations were described in a previous report [15].

Fully developed turbulent flat plate boundary layer flow properties were used as the upstream boundary conditions at $X/\delta_o = 0$. These boundary flow properties were first calculated by using the computational code. The turbulent flat plate 1/7th power law velocity profile was assumed for the initial stream-wise mean velocity components. The initial normal direction mean velocity components were set to zero. The velocity and temperature relationship of a compressible laminar boundary layer along a heated flat plate [15] was used to define the initial mean temperature distributions. The far-field boundary conditions were prescribed by the free-stream conditions. The no-slip condition, constant wall temperature, and zero normal pressure gradient were used for the wall boundary conditions. It was further assumed that the flow properties did not change along the external mean velocity direction. With this assumption, zero property gradients along the X-direction were used as the upstream and downstream boundary conditions. The physical computational domain for establishing the flat plate boundary layer conditions was 7.5 δ_o in the X-direction and 2 δ_o in the Y-direction. An H-type grid with a 40 by 149 mesh size was used in the computations. The grid points were packed near the wall along the Y-direction. However, the grid points were uniformly distributed along the X-direction. For the k and ε computations, the incompressible flat plate boundary layer turbulent kinetic energy [16] was used as the initial conditions of k. The initial dissipation rate was calculated by using $\varepsilon = \rho C_\mu k^2 / \mu_t$ where μ_t was obtained from the Baldwin-Lomax turbulence model computations.

The computed turbulent flat plate boundary layer flow properties were used both as the upstream boundary conditions and the initial conditions of the Navier-Stokes computations of the compression ramp flows. The physical domain was chosen such that the reflected shock wave crossed the downstream out-flow boundary and ,therefore, the free-stream properties were used as the far-field boundary conditions. With the present free-stream conditions, the 8° and 16° compression ramps induced slightly different reflected shock wave orientations. Consequently, two different physical domains were chosen respectively for the 8° and 16° compression ramp flow computations. A domain of 7 δ_o in the X-direction and 2 δ_o in the Y-direction was used for the 8° compression ramp computation, and a domain of 7.5 δ_o in the X-direction and 2.5 δ_o in the Y-direction was used for the 16° compression ramp computations. The flow properties at the out-flow boundary were also assumed to remain constant along the downstream free stream direction. An H-type grid with a 221 by 149 mesh size was used for the present computations.

A general concept [15] of the transformation between the physical and the computational domains was also used in the present computations. The transformation was required to concentrate the computational mesh points within the near wall and the corner regions where large gradients in the flow properties would occur. Two different grid configurations were used previously [8] for the 8° and 16° compression ramp flow computations. These grid configurations were optimized, by changing the packing parameters [15], to obtain satisfactory computational results of the Reynolds shear stresses. These grid configurations were also used here. Using the computed flat plate boundary layer flow properties as the initial conditions, the numerical computation, with a CFL number = 0.4, required approximately 45,000 time iterations to obtain a steady state solution. The computation process was time consuming.

RESULTS AND DISCUSSIONS

Based on the turbulence modeling techniques, some of the computational results of the flow properties, such as the turbulent eddy viscosity, the Reynolds shear stress, the stream-wise mean flow velocity, and the surface heat transfer rate, are described and discussed in the following sections. To assess the accuracy of the present computations, the computational results are also compared with similar results from experiments [5, 10, and 11].

Upstream Flat Plate Boundary Layer Flow Properties

The computed Reynolds shear stress profiles, at $X/\delta_o = 0.5$ location, with the standard and modified Baldwin-Lomax turbulence models are shown in Fig. 3(a). A constant Reynolds analogy factor, $S = 1$, was used at this X-location in the computations. The computational results are also compared with existing Reynolds shear stresses measurements [10]. Both models predicted approximately the Reynolds shear stress variation. The standard Baldwin-Lomax model calculated larger Reynolds shear stresses at locations away from the wall surface. By changing the value of C_{kleb} from 0.3 [6] to 0.8, the modified model could predict the experimental Reynolds shear stresses at the locations away from the wall surface. Thus, a different intermittency factor is required to use the Baldwin-Lomax model for supersonic boundary layer Reynolds shear stress computation.

The computed Reynolds shear stress profiles at $X/\delta_o = 0.5$ from the computations with low-Reynolds-number and hybrid $k-\varepsilon$ turbulence models were plotted and compared with the measurements in Fig. 3(b). The computational results agree very well with the measurements. Particularly noteworthy, these turbulence modeling techniques could describe the near wall Reynolds shear stress variation as it was shown by the experimental results.

The present computational results of the boundary layer mean velocity profile at $X/\delta_o = 0.5$ were studied, using an existing compressible boundary layer flow analysis [17]. This existing analysis used a transformation theory [18] to map the compressible turbulent boundary layer flow velocity profile into an incompressible flow law of the wall velocity correlation. A brief description of the mapping technique was presented in the APPENDIX of the paper. This mapping technique was used to correlate the Y-directional variations of the velocity component, U, and density, ρ, from the present computations. The mapping process leads to the prediction of the skin friction factor. This skin friction factor can be compared with the skin friction factor obtained from the computations. The experiments [11] measured the flat plate boundary layer velocity and Mach

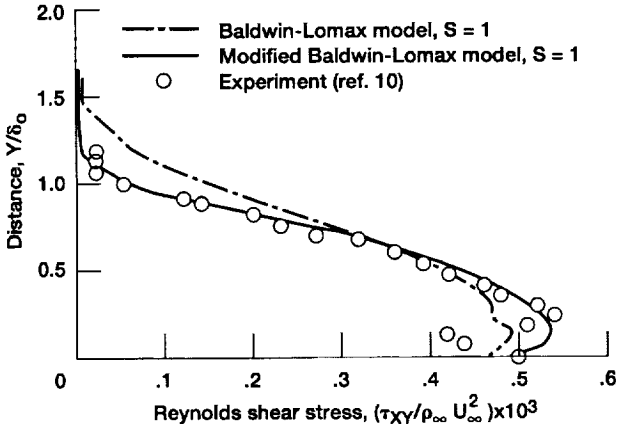

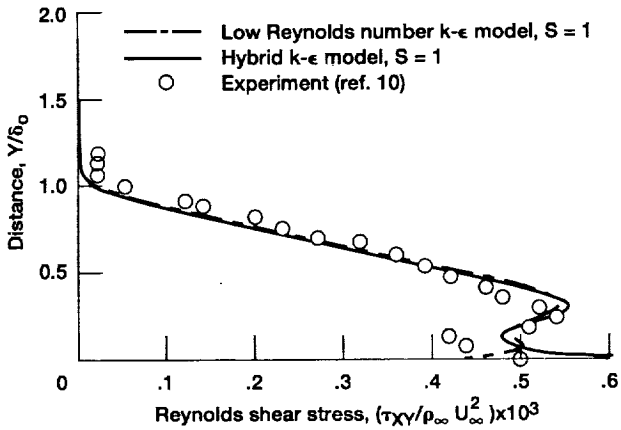

Figure 3.—Upstream Reynolds shear stress profiles, $X/\delta_O = 0.5$.

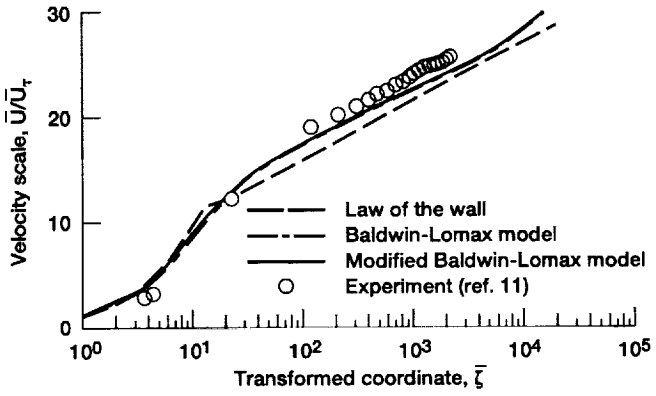

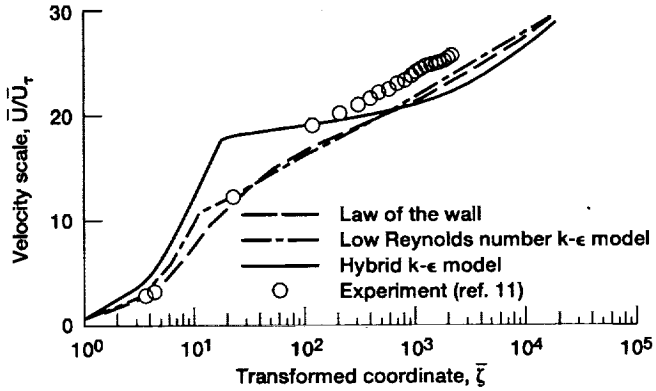

Figure 4.—Law of the wall velocity profiles, $x/\delta_O = 0.5$.

number profiles. Assuming an adiabatic wall condition, we calculated the boundary layer density variation based on the experimental Mach number profile. The mapping technique was then used to correlate the velocity component, U, and the density, ρ. This correlation was then compared with the correlation based on the present Navier-Stokes computational results of U and ρ. The law of the wall, in terms of the velocity scale, $\overline{U} / \overline{U}_\tau$, and the transformed coordinate, $\overline{\zeta}$, are shown in Figs. 4(a) and (b). Using the Baldwin-Lomax models, the computations predicted larger $\overline{U} / \overline{U}_\tau$ than that was prescribed by the law of the wall (Fig. 4(a)). Using the $k-\varepsilon$ turbulence model, the computations predicted a smaller $\overline{U} / \overline{U}_\tau$ than that was prescribed by the law of the wall (Fig. 4(b)). Using the hybrid $k-\varepsilon$ turbulence model, the present computations predicted large $\overline{U} / \overline{U}_\tau$ at locations near the viscous sublayer edge (Fig. 4(b)) and failed to resolve the velocity profile within the buffer layer. This may be because the model did not consider the turbulence modeling within the buffer layer. Despite this, the hybrid $k-\varepsilon$ model generally does a good job of describing the flow properties. A value, $\overline{C}_f = 0.002$, for the incompressible skin friction factor was required to establish the correlations from the present computational results of the velocity component, U, and the density, ρ. Based on this $\overline{C}_f$ value, Eq. (A5) gives $C_f = 0.001$. The present computations also predicted a skin friction factor, $C_f = 0.0009$. In addition, the computations calculated a surface heat transfer rate, $Q_w = 0.75$ Btu / ft^2 – sec, for a near adiabatic wall condition, $T_w / T_{o,\infty} = 1.04$. The above observations indicated that the present Navier-Stokes computations could predict the surface heat transfer and the skin friction factor.

As it was shown by the results in Figs. 4(a) and (b), the experimental data agrees well with the law of the wall for $\overline{\zeta} < 10.6$. For $\overline{\zeta} > 10.6$, the experiment shows a larger velocity scale than that was calculated by using Eq. (A1). With the Baldwin-Lomax model for turbulence modeling, the computational velocity (Fig. 4(a)) agrees closely with the experimental data. With the $k-\varepsilon$ turbulence transport equations for turbulence modeling, the computational velocity correlations (Fig. 4(b)) show a lower velocity scale than that was indicated by the experimental data. At large $\overline{\zeta}$ locations, the computations also predicted a lower $\overline{U} / \overline{U}_\tau$ than that was given by Eq. (A1).

The present computational results of the eddy viscosity from different turbulence models were also plotted in terms of the transformed coordinate $\overline{\zeta}$ in Figs. 5(a) and (b). The modified Baldwin-Lomax model (with $C_{kleb} = 0.8$) calculates small eddy viscosity at the location away from the surface (Fig. 5(a)) and this model predicts the experimental measurements of the Reynolds shear stress (Fig. 3(a)). The low-Reynolds-number $k-\varepsilon$ turbulence model and the hybrid $k-\varepsilon$ model calculate approximately the same eddy viscosities within most parts of the boundary layer (Fig. 5(b)). A difference in the eddy viscosities occurs only at locations very close to

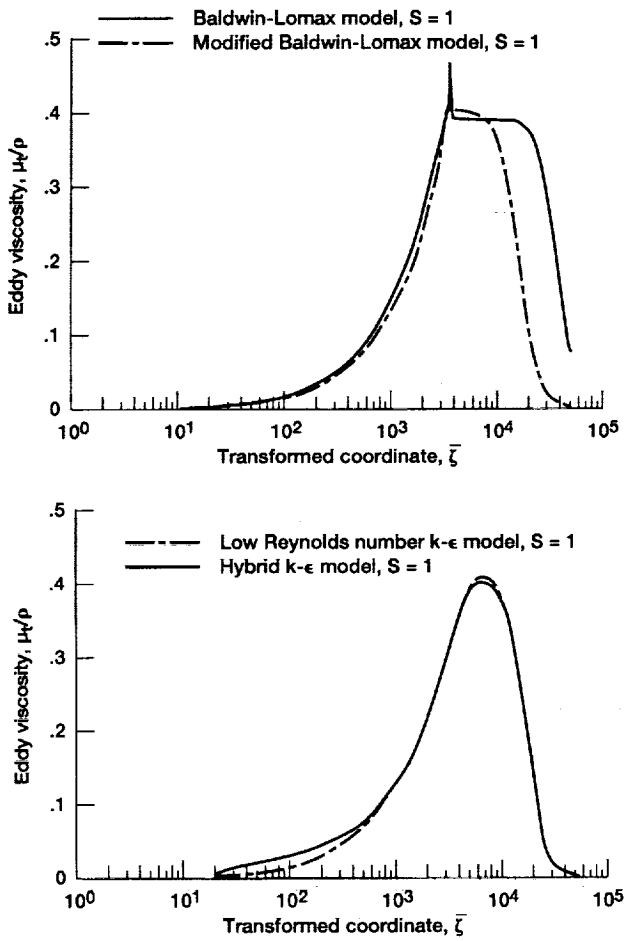

Figure 5.—Upstream eddy viscosity profiles, $x/\delta_o = 0.5$.

the surface. These $k-\varepsilon$ models only induce differences in the Reynolds shear stress predictions at the near surface locations (Fig. 3(b)). A comparison between the results of eddy viscosity in Figs. 5(a) and (b) also reveals that both the $k-\varepsilon$ models predicted approximately the eddy viscosity as it was calculated by using the modified Baldwin-Lomax eddy viscosity model. This also verifies that the Baldwin-Lomax eddy viscosity formulation requires $C_{kleb} = 0.8$ in order to model the turbulent momentum flux of a supersonic boundary layer flow.

8 Degree Compression Ramp Downstream Flow Properties

The computed Reynolds shear stress profiles, based on the standard and modified Baldwin-Lomax turbulence models and the hybrid $k-\varepsilon$ models, at five different X/δ_o locations were shown in Fig. 6. A constant Reynolds analogy factor, $S_u = S_d = 1$, was used in the computations. The computational results were also compared with the experimental measurements [10]. The standard Baldwin-Lomax model predicted lower downstream $\tau_{XY}/\rho_\infty U_\infty^2$ values than were measured. With $C_i = 0.45$ and $C_{kleb} = 0.8$, the modified model could predict accurately the Reynolds shear stress distributions downstream of the shock wave. The present computations also required a larger C_i value to account for the downstream Reynolds shear stress amplification. Based on the hybrid $k-\varepsilon$ turbulence modeling techniques, the computed Reynolds shear stresses also agreed well with their measurements especially at the downstream locations. Both the computation and the experiment gave downstream Reynolds shear stress profiles which are significantly different from the profile at upstream location. Along the Y-direction and near the shock wave locations, the computed Reynolds shear stress increases and then decreases to its free stream condition. However, the measurements indicate that, near the shock wave locations, τ_{XY} reduces and then increases to its free stream value.

The computed surface pressure, p_w/p_∞, and the skin friction factor, $C_f = \tau_w/(1/2)\rho_\infty U_\infty^2$, variations are shown in Fig. 7. The surface shear stress was computed by using $\tau_w = \mu_w \left.\frac{\partial U_s}{\partial n}\right|_w$. The velocity components U and V were used to obtain numerically the normal velocity gradient, $\left.\frac{\partial U_s}{\partial n}\right|_w$, at the wall surface. At an upstream location ($X \le X_c$), the velocity gradient, $\left.\frac{\partial U_s}{\partial n}\right|_w = \left.\frac{\partial U}{\partial Y}\right|_w$, was evaluated based on the U values at the first three grid points from the surface. At a downstream location ($X > X_c$), U and V at the first three grid points were first used to determine the velocity components U_s at the grid points. These velocity components were then used to evaluate numerically the normal velocity gradient, $\left.\frac{\partial U_s}{\partial n}\right|_w$. The experimental results [10] of these surface conditions were also plotted in Fig. 10 for comparison. Using either Baldwin-Lomax turbulence model, the computations predicted the experimental surface pressure distribution. Using the modified Baldwin-Lomax model, the computations calculated a higher level of the skin friction downstream of the compression corner. This skin friction distribution agrees better with the measurements. Using the hybrid $k-\varepsilon$ model, the computations could also predict accurately both the experimental surface pressure and skin friction variations.

16 Degree Compression Ramp Downstream Flow Properties

Using the best turbulence models for the 8° ramp and the Reynolds analogy assumptions, the computed Reynolds shear stress variations along the Y-direction at five different X/δ_o locations were shown in Figs. 8(a) and (b). For comparisons, the corresponding shear stress measurements [10] were also plotted in Figs. 8(a) and (b). Figure 8(a) shows these results when the modified Baldwin-Lomax model and different Reynolds analogy assumptions were used respectively in the computations. With constant Reynolds analogy factor, $S_u = S_d = 1$, the computations well predicted the experimental Reynolds shear stress variations along the Y-direction at $X/\delta_o = 5.5$ and 6.5 locations. However, the computed Reynolds shear stresses, at the near corner locations, were larger then the measured Reynolds shear stresses. With the experimental Reynolds analogy factor, $S_d = 3.65 - (X/\delta_o - 2.5)^{0.38}$, the computations overpredicted the Reynolds shear stresses at almost all downstream

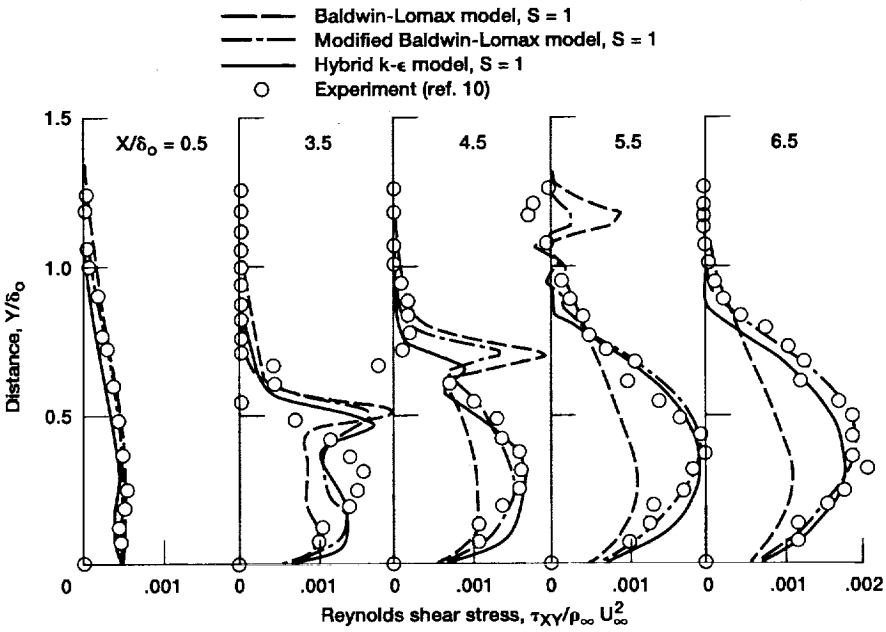

Figure 6.—Reynolds shear stress profiles, θ = 8°.

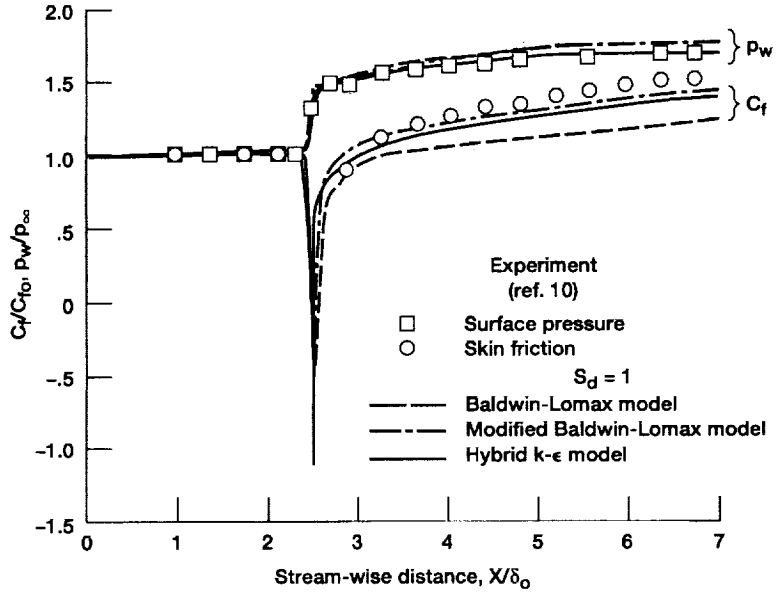

Figure 7.—Surface pressure and skin friction factor of θ = 8°.

locations. Figure 8(b) presented the results when the hybrid $k-\varepsilon$ turbulence model and different Reynolds analogy assumptions were used in the computations. The computations, using $S_u = S_d = 1$, computed approximately the experimental Y-directional shear stress profile at $X / \delta_o = 3$ location. Using either $S_d = 1$ or $S_d = 2$ in the computations, the computations could predict the shear stress variation along the Y-direction at $X / \delta_o = 6.5$ location. Changing the S_d value from 1 to 2 in the computations, the computations produced small differences in the Reynolds shear stress predictions.

The computed skin friction factor and surface pressure variations, with different turbulence models and the Reynolds analogy factor assumptions, were plotted and compared with their experimental measurements [10] in Figs. 9(a) and (b). The computational results of the skin friction factor were obtained in a manner as it was used in the 8° compression ramp flow calculations. These results indicated that the downstream Reynolds analogy assumption did not significantly affect the present computations of the surface pressure and skin friction factor. Using the modified Baldwin-Lomax

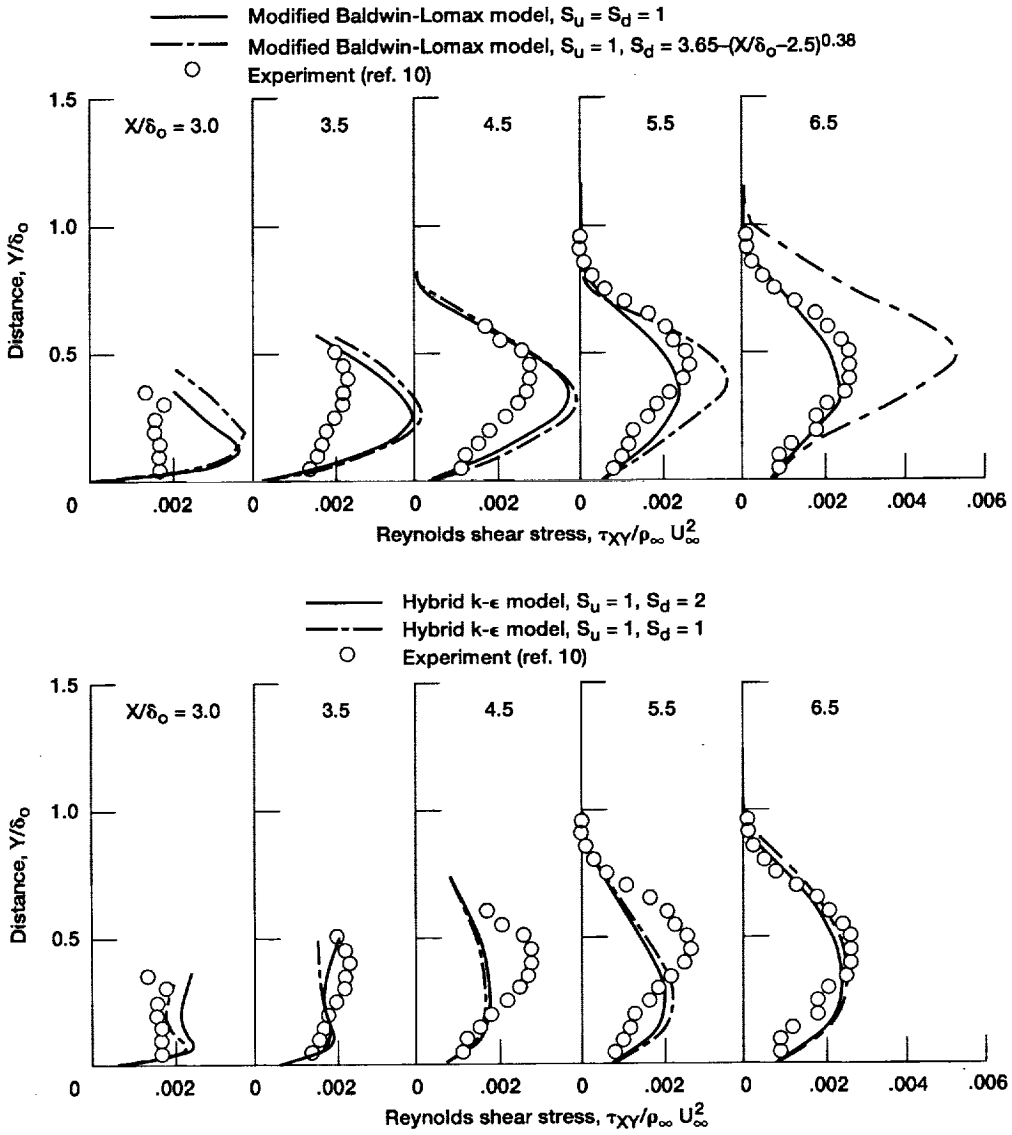

Figure 8.—Reynolds shear stress profiles, $\theta = 16°$.

model (Fig. 9(a)), the computations closely predicted the surface pressure but poorly predicted the skin friction factors. The computational results of the skin friction factor indicated that flow separation occurred near the corner location. Just the opposite was true, using the hybrid $k-\varepsilon$ turbulence model (Fig. 9(b)), the computations calculated a lower level of the downstream surface pressure and accurately predicted the skin friction factor variation. The computational results of the skin friction factor also indicated that a very small flow separation region existed around the corner location. This is close to the experimental observation [10] that incipient flow separation could occur near the corner location.

For a compression ramp flow, it has been shown [19] that the upstream and downstream static pressure ratio played an important role in modifying the turbulence within the flow field. The role of the pressure ratio was not included in the hybrid $k-\varepsilon$ turbulence model. It could not capture fully the turbulence distortion in the compression ramp flow and the present computation could not predicted accurately the surface pressure on the 16°compression ramp. The success of the present calculation of the skin friction along the 16° ramp may require further investigation. However, the hybrid $k-\varepsilon$ turbulence model is straightforward and is a worthwhile advancement for the engineering application.

The Navier-Stokes computational results of the static temperatures at the first three grid points from the wall surface were used to calculate numerically the normal temperature gradient, $\left.\frac{\partial T}{\partial n}\right|_w$ at the wall surface. This temperature gradient was then used to compute the surface heat transfer rate by using $Q_w = -K_w \left.\frac{\partial T}{\partial n}\right|_w$. The com-

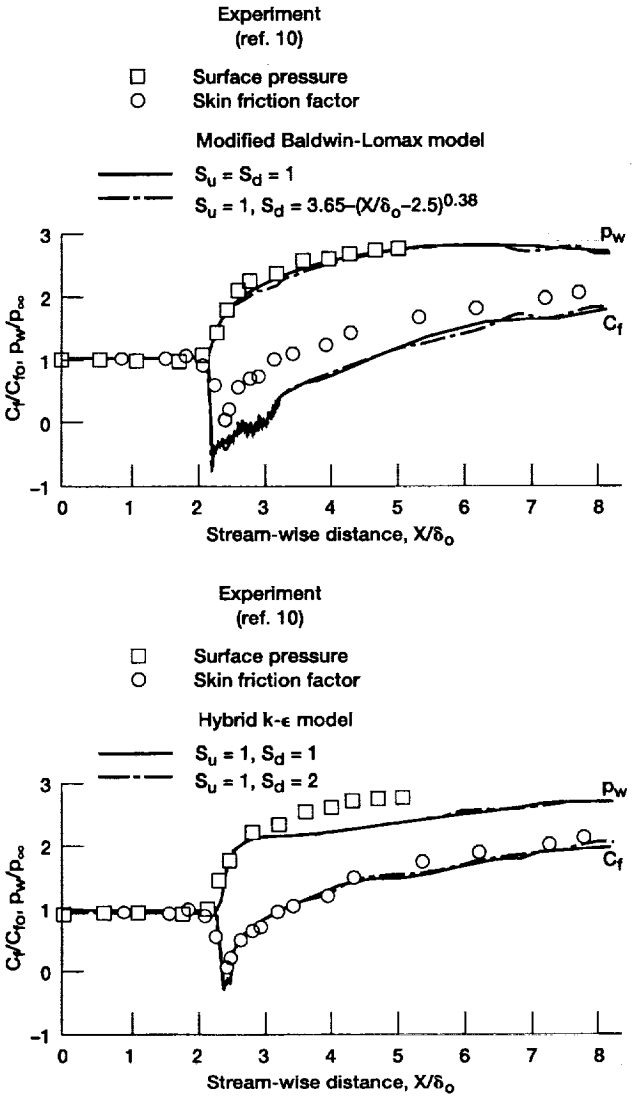

Figure 9.—Surface pressure and skin friction factor, θ = 16°.

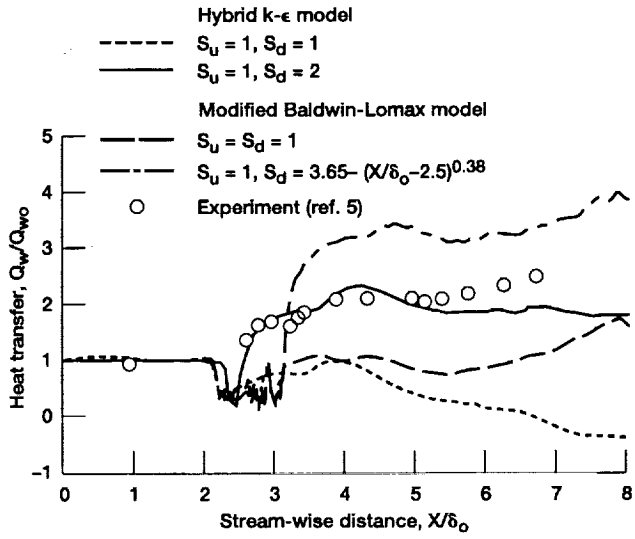

Figure 10.—Surface heat transfer distribution, θ = 16°.

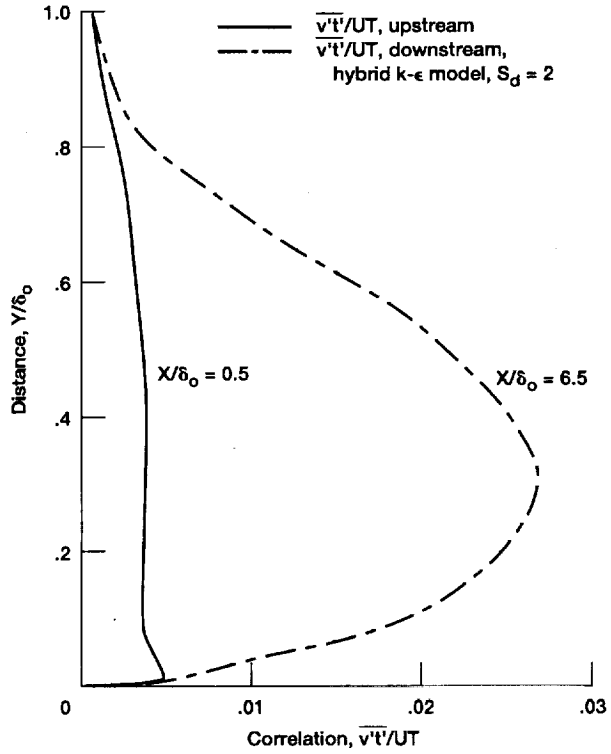

Figure 11.—Correlations of velocity and temperature fluctuations, θ = 16°.

puted surface heat transfer results, based on different assumptions of the Reynolds analogy factor and turbulence models, were plotted and compared with the measurements [5] in Fig. 10. With constant Reynolds analogy factor, $S = 1$, the computational results did not show significant increase in the surface heat transfer at the downstream locations. With the experimental Reynolds analogy factor and the modified Baldwin-Lomax turbulence model, the computed surface heat transfer rate decreased at locations just upstream of the corner location. The surface heat transfer rate oscillated at locations immediately downstream of the corner and, then, increased rapidly to a higher value than that was measured. Using the hybrid $k-\varepsilon$ turbulence model and $S_u = S_d = 1$ assumption, the computations even predicted a reduction in the surface heat transfer at the downstream locations. However, using a $S_d = 2$ assumption, the computation predicted the downstream surface heat transfer variation. A turbulent Prandtl number $Pr_t = 0.93$ was used in the computations. Thus, the combination of the hybrid $k-\varepsilon$ turbulence model and a ratio of $\mu_q / \mu_l = 2.15$ seems to be an appropriate turbulence modeling technique for the computations of the surface heat transfer rate downstream of the 16° compression ramp.

It should be noted that for one case, the case with $S_u = 1$ and $S_d = 3.65-(X/\delta_o-2.5)^{0.38}$ assumptions and the modified

Baldwin-Lomax turbulence model for 16° ramp, only preliminary computational results are described in this paper. Because of the very long computing time, we used the previously computed 8° compression ramp mean flow properties to start this part of computations. The computational results did not show significant variations after 15,000 time iterations. Thus, the computational results, at the 15,000th iteration, were presented in Figs. 8(a), 9(a), and 10.

Equations (15), (16), and (21) were used to model the turbulent heat flux terms for the present computational analysis. The 16° compression ramp computations (with $S_u = 1$ and $S_d = 2$) indicated the turbulent heat flux $\overline{v't'} / UT$ changed significantly as flow moved downstream. For example, the computed profiles of the $\overline{v't'} / UT$ correlation at the upstream $\left(X / \delta_o = 0.5\right)$ and the downstream $X / \delta_o = 6.5$ locations were plotted in Fig. 11. These profiles indicated that, within the boundary layer flow, the correlation $\overline{v't'} / UT$ was amplified at the downstream location.

Recently, advanced turbulence modeling techniques have been developed to model the near wall turbulence. Turbulence transport equations [20] were used to analyze the near wall turbulent heat flux. The turbulence modeling techniques could calculate the velocity-temperature correlations within some incompressible boundary layer flows. An analysis [21] was also proposed to relate the evolution of the Reynolds stress and the turbulent heat flux to the mean flow properties in a shock-wave/turbulence interaction. These new turbulence modeling techniques may lead to a better analytical approach for the predictions of the Reynolds shear stress, the turbulent heat flux, and the surface heat transfer rate of a shock-wave/turbulent boundary layer interaction flow field.

CONCLUSIONS

The application of turbulence modeling techniques and the Reynolds analogy in the Navier-Stokes computations of two-dimensional supersonic compression ramp flows were investigated. The Baldwin-Lomax eddy viscosity concept and the $k-\varepsilon$ turbulence models (with and without modifications) were used for turbulent momentum flux modeling. The Reynolds analogy was used for the turbulent thermal flux modeling. The ratio of the thermal and momentum transport coefficients was assumed to be S/Pr_t. S is an analogy factor and it was also assumed to be a function of the streamwise location. The turbulent Prandtl number is constant, $\mathrm{Pr}_t = 0.93$. The Navier-Stokes equations and the energy equation were solved numerically for the flow properties of the compression ramp flow field. The Reynolds shear stress, skin friction factor, and the surface heat transfer rate were calculated and compared with their measurements. It was concluded that:

(a) The Navier-Stokes computations predicted the supersonic flat plate boundary layer flow properties when the k and ε transport equations were used for turbulence modeling of a boundary layer flow with nonadiabatic wall condition.

(b) A modified Baldwin-Lomax turbulence model and a hybrid $k-\varepsilon$ turbulence model were found to be effective for the Navier-Stokes computations of the Reynolds shear stress and the skin friction of a supersonic compression ramp flow. The ratio of the transport coefficients in the Reynolds analogy only slightly influenced the computations of the Reynolds shear stress, the skin friction factor, and the surface pressure.

(c) The ratio of the transport coefficients used in the Reynolds analogy has an impact on the computation of the surface heat transfer rate downstream of the compression ramp. With a transport coefficient ratio of $2/\mathrm{Pr}_t$ and a hybrid $k-\varepsilon$ turbulent momentum flux modeling technique, the present computations predicted the experimental results of the heat transfer rate on a 16° compression ramp surface.

APPENDIX

Baronti and Libby [17] performed an analysis to map a compressible turbulent boundary layer flow into an incompressible boundary layer flow. Their results showed that the compressible flow velocity profile was well correlated by the law of the wall. The law of the wall was written as

$$\overline{U} / \overline{U}_\tau = \overline{\zeta}, \quad \text{for} \quad 0 < \overline{\zeta} \le \overline{\zeta}_f$$

$$= 2.43 \ln 7.5\overline{\zeta}, \quad \text{for} \quad \overline{\zeta}_f < \overline{\zeta} \tag{A1}$$

where $\overline{U}_\tau = \left(\overline{\tau}_w / \rho_w\right)^{0.5}$ is frictional velocity. $\overline{\zeta}_f = 10.6$ was assumed. The Y-directional transformed coordinate, $\overline{\zeta}$, was defined as

$$\overline{\zeta} = \left(\frac{\overline{C}_f}{2}\right)^{0.5} \left(\frac{\mu_\infty \sigma}{\mu}\right) \left(\frac{\rho_\infty U_\infty}{\mu_\infty}\right) \int_o^Y \left(\frac{\rho}{\rho_\infty}\right) dY \tag{A2}$$

with

$$\left(\frac{\mu_\infty \sigma}{\mu}\right) = \left(\frac{\rho_f}{\rho_\infty}\right) \left(\frac{\mu_\infty}{\mu_f}\right) \overline{\zeta}_f \int_o^{\overline{\zeta}_f} \left(\frac{\rho_\infty}{\rho}\right) d\overline{\zeta} \tag{A3}$$

Some relationships between the compressible and incompressible flow properties were also written as

$$\frac{\overline{U}}{\overline{U}_\tau} = \left(\frac{U_\infty}{U}\right) \left(\frac{\overline{C}_f}{2}\right)^{0.5} \tag{A4}$$

and

$$\overline{C}_f = \left(\frac{\rho_\infty \mu_\infty}{\rho_w \mu_w}\right) \left(\frac{\mu}{\sigma \mu_\infty}\right) C_f \tag{A5}$$

Given a $\overline{C}_f$ value and the compressible flow velocity and density profiles, Eqs. (A2) to (A4) could be used to calculate $\overline{U} / \overline{U}_\tau$ and $\overline{\zeta}$ at a specific Y location. It is also possible to select a value of $\overline{C}_f$ which correlates $\overline{U} / \overline{U}_\tau$ and $\overline{\zeta}$ in the law of the wall region. Based on the $\overline{C}_f$ value, Eq. (A5) could then be used to calculated compressible flow skin friction factor C_f.

REFERENCES

1.Delery, J.; Marvin, J.G.; and Reshotko, E.: Shock-Wave Boundary Layer Interactions. AGARD AG–280, 1986.

2.Horstman, C.C.: Prediction of Hypersonic Shock-Wave/Turbulent-Boundary Layer Interaction flows. AIAA Paper 87–1367, 1987.

3.Coakley, T.J.; and Huang, P.G.: Turbulence Modeling For High Speed Flows. AIAA Paper 92–0436, 1992.

4.Schlichting, H.: Boundary Layer Theory. Sixth Edition, McGraw-Hill, 1968, pp. 660–661.

5.Evans, T.T.; and Smits, A.J.: Measurements of the Mean Heat Transfer in a Shock Wave Turbulent Boundary Layer Interaction. Presented at the Thirteenth Symposium on Turbulence, University of Missouri-Rolla, Sept. 21–23, 1992.

6.Baldwin, B.; and Lomax, H.: Thin-Layer Approximation and Algebraic Model for Separated Turbulent Flows. AIAA Paper 78–257, 1978.

7.Nichols, R.H.: A Two-Equation Model for Compressible Flows. AIAA Paper 90–0494, 1990.

8.Wang, C.R.: Supersonic Boundary-Layer Flow Turbulence Modeling. Near-Wall Turbulent Flows, Elsevier Publishers, 1993, pp. 219–228.

9.Shang, J.S.; Hankey, W.L.; and Law, C.H.: Numerical Simulation of Shock Wave-Turbulent Boundary-Layer Interaction. AIAA J., Vol. 14, No. 10, Oct. 1976, pp. 1451–1457.

10.Smits, A.J.; and Muck, K.C.: Experimental Study of The Shock Wave/Turbulent Boundary Layer Interaction. J. Fluid Mechanics, Vol. 182, 1987, pp. 291–314.

11.Muck, K.C.; Spina, E.F.; and Smits, A.J.: Compilation of Turbulence Data for an 8° Compression Corner at Mach 2.9. Department of Mechanical and Aerospace Engineering, Princeton University, Rept. MAE–1642, Apr. 1984.

12.Gorski, J.J.: A New Near-Wall Formulation for the k-ε Equations of Turbulence. AIAA Paper 86–0556, 1986.

13.Goldberg, U.C.: Separated Flow Treatment with a New Turbulence Model. AIAA J., Vol. 24, No. 10, Oct. 1986, pp. 1711–1713.

14.MacCormack, R.W.: The Effect of Viscosity in Hypervelocity Impact Cratering. AIAA Paper 69–354, 1969.

15.Wang, C.R.; Hingst, W.R.; and Porro, A.R.: Heat Transfer, Velocity-Temperature Correlation, and Turbulent Shear Stress from Navier-Stokes Computations of Shock Wave/Turbulent Boundary Layer Interaction Flows. NASA CP–3078, pp. 429–456, 1990.

16.Klebanoff, P.S.: Characteristics of Turbulence in a Boundary Layer with Zero Pressure Gradient. NACA TN–3178, 1955.

17.Baronti, P.O.; and Libby, P.A.: Velocity Profiles in Turbulent Compressible Boundary Layers. AIAA J., Vol. 4, No. 2, 1968, pp. 193–202.

18.Crocco, L.: Transformation of the Compressible Turbulent Boundary Layer with heat exchange. AIAA J., Vol.1, 1963, pp. 2723–2731.

19.Smits, A.J.; and Wood, D.H.: The Response of Turbulent Boundary Layers to Sudden Perturbation. Ann. Rev. Fluid Mech. 17, pp. 321–358, 1985.

20.Lai, Y.G.; and So, R.M.C.: Near Wall Modeling of Turbulent Heat Fluxes. International Journal of Heat and Mass Transfer, Vol. 33, pp. 1429–1440, 1990.

21.Debieve, J.E.; Gouin, H.; and Gaviglio, J.: Momentum and Temperature Fluxes in a Shock-Wave Turbulence Interaction. Preceding of ICHMT/IUTAM Symposium on the Structure of Turbulence and Heat and Mass Transfer, Hemisphere Publishing Co., Washington, DC, pp. 277–296, 1980.

REPORT DOCUMENTATION PAGE

Form Approved
OMB No. 0704-0188

1. AGENCY USE ONLY (*Leave blank*)	2. REPORT DATE	3. REPORT TYPE AND DATES COVERED
	January 1994	Technical Memorandum

4. TITLE AND SUBTITLE

Turbulence Models and Reynolds Analogy for Two-Dimensional Supersonic Compression Ramp Flow

5. FUNDING NUMBERS

WU–505–62–52

6. AUTHOR(S)

Chi R. Wang and Maleina C. Bidek

7. PERFORMING ORGANIZATION NAME(S) AND ADDRESS(ES)

National Aeronautics and Space Administration
Lewis Research Center
Cleveland, Ohio 44135–3191

8. PERFORMING ORGANIZATION REPORT NUMBER

E–8349

9. SPONSORING/MONITORING AGENCY NAME(S) AND ADDRESS(ES)

National Aeronautics and Space Administration
Washington, D.C. 20546–0001

10. SPONSORING/MONITORING AGENCY REPORT NUMBER

NASA TM–106474

11. SUPPLEMENTARY NOTES

Prepared for the 1994 Thermophysics and Heat Transfer Conference sponsored by the American Society of Mechanical Engineers, Colorado Springs, Colorado, June 20–23, 1994. Chi W. Wang, NASA Lewis Research Center and Maleina C. Bidek, Cornell University, Department of Computer Science, Ithaca, New York 14853, and Student Intern at NASA Lewis Research Center. Responsible person, Chi R. Wang, organization code 2630, (216) 433–5865.

12a. DISTRIBUTION/AVAILABILITY STATEMENT

Unclassified - Unlimited
Subject Category 34

12b. DISTRIBUTION CODE

13. ABSTRACT ***(Maximum 200 words)***

We present results of the application of turbulence models and the Reynolds analogy to the Navier-Stokes computations of Mach 2.9 two-dimensional compression ramp flows. We studied the Baldwin-Lomax eddy viscosity model and the k-ε turbulence transport equations for the turbulent momentum flux modeling in the Navier-Stokes equations. We also studied the Reynolds analogy for the turbulent heat flux modeling in the energy equation. The Navier-Stokes equations and the energy equation were numerically solved for the flow properties. The Reynolds shear stress, the skin friction factor, and the surface heat transfer rate were calculated and compared with their measurements. We concluded that (a) with a hybrid k-ε turbulence model for turbulence modeling, the present computations predicted the skin friction factors of the 8° and 16° compression ramp flows and (b) with the turbulent Prandtl number $Pr_t = 0.93$ and the ratio of the turbulent thermal and momentum transport coefficients $\mu_q/\mu_t = 2/Pr_t$, the present computations also predicted the surface heat transfer rates beneath the boundary layer flow of the 16 compression ramp.

14. SUBJECT TERMS

Heat transfer; Turbulence; Boundary layer flow

15. NUMBER OF PAGES
15

16. PRICE CODE
A03

17. SECURITY CLASSIFICATION OF REPORT	18. SECURITY CLASSIFICATION OF THIS PAGE	19. SECURITY CLASSIFICATION OF ABSTRACT	20. LIMITATION OF ABSTRACT
Unclassified	Unclassified	Unclassified	